Front. Earth Sci. 2018, 12(4): 818–833
https://doi.org/10.1007/s11707-018-0697-9

RESEARCH ARTICLE

The effects of air temperature and precipitation on the net primary productivity in China during the early 21st century

Qianfeng WANG[1,2,3], Jingyu ZENG[1,2,3], Song LENG[4], Bingxiong FAN[1,2,3], Jia TANG[1,2,3], Cong JIANG[5], Yi HUANG[1,2,3], Qing ZHANG[6], Yanping QU[7,8], Wulin WANG[1,2,3], Wei SHUI (✉)[1,2,3]

1 College of Environment and Resource, Fuzhou University, Fuzhou 350116, China
2 Key Laboratory of Spatial Data Mining & Information Sharing, Ministry of Education of China, Fuzhou 350116, China
3 Fujian Provincial Key Laboratory of Remote Sensing of Soil Erosion and Disaster Protection, Fuzhou 350116, China
4 Climate Change Cluster, University of Technology Sydney, Broadway, New South Wales 2007, Australia
5 College of Biological Science and Engineering, Fuzhou University, Fuzhou 350116, China,
6 Key Laboratory of Digital Earth Science, Institute of Remote Sensing and Digital Earth, Chinese Academy of Sciences, Beijing 100094, China
7 China Institute of Water Resources and Hydropower Research, Beijing 100038, China
8 Research Center on Flood and Drought Disaster Reduction, Beijing 100038, China

Abstract Research on how terrestrial ecosystems respond to climate change can reveal the complex interactions between vegetation and climate. net primary productivity (NPP), an important vegetation parameter and ecological indicator, fluctuates within any given ecological environment or regional carbon budget. In this study, spatial interpolation was used to generate a spatial dataset, with 1-km spatial resolution, with meteorological data from 736 observation stations across China. An improved CASA model was used to simulate NPP over the period of 2001–2013 by taking into account land-cover change in every year during the same period. We propose the grid-based spatial patterns and dynamics of annual NPP, annual average temperature, and annual total precipitation based on the model. We also used the model to demonstrate the spatial correlation between NPP, temperature, and precipitation in the study area with special focus on the impact of climate change in the early 21st century. Results showed that the spatial pattern of NPP over all of China is characterized by higher values in the southeast and lower values in the northwest. The spatial pattern of temperature indicates substantial latitudinal differences across the country, and the spatial pattern of precipitation shows a ribbon of decline from the southeast coast to the northwest inland. Most areas show an upward trend in NPP. Temperatures appear to decrease across the country during the global warming hiatus (1998–2008), and are accompanied by an increase in precipitation over most regions. The correlation between NPP and annual average temperature is weak. Alternatively, NPP and annual total precipitation are positively correlated in northern and central China at a coefficient above 0.64 ($p < 0.01$) yet negatively correlated in the eastern parts of the Qinghai-Tibet Plateau and Sichuan Basin. Results can provide useful information for improving parameters for calibration of the terrestrial ecosystem process model.

Keywords impact, air temperature, precipitation, NPP, China

Received July 26, 2017; accepted December 18, 2017

E-mail: shuiwei@fzu.edu.cn

1 Introduction

The interaction between climate change and terrestrial ecosystems has long been considered one of the key fields of ecological research. Climate variables, especially temperature and precipitation, are the main factors influencing the evolution and scope of our world's ecosystems (Gang et al., 2017). The global climate has transformed continually since the industrial revolution as a result of anthropogenic activities such as the spike in greenhouse gas emissions (namely CO_2) from fossil fuel combustion (Chandrappa et al., 2011). According to the Fourth Assessment Report of the United Nations Intergovernmental Panel on Climate Change (IPCC), the concentration of atmospheric CO_2 has increased from about 280 ppm in the mid-1900s to 379 ppm in 2005, in other words, more than 30% over the past century (Pachauri et al., 2014). An increase of 1.9°C–5.2°C, presumably around 4°C, is anticipated in the global surface

average temperature during the next century. A 5%–20% increase in annual total precipitation, with regional differences in precipitation trends (Palut and Canziani, 2007) is also expected. All of these changes would have a significant impact on the net primary productivity (NPP) of terrestrial vegetation, leading to a series of combined effects on global society (Nemani et al., 2003). The Earth's surface experienced tremendous environmental changes from 1980 to 2000 (Yu et al., 2008). The terrestrial NPP of China has been particularly affected by global climate change (Cao and Woodward, 1998; Olesen et al., 2007; Dong and Yu, 2008; Piao et al., 2008). The recent dynamic responses of NPP to temperature and precipitation, arguably the important indicators of climate change, have crucial research significance in the ecological field. NPP, one of the key indicators of ecosystem function (Running et al., 2004; Crabtree et al., 2009), refers to the amount of chemical energy as biomass that plants create through photosynthesis per unit area per unit of time, excluding the energy expended for respiration. NPP is used to measure or estimate the amount of carbon fixed by the synthesis of organic compounds from atmospheric carbon dioxide via photosynthesis. It is also used to evaluate carbon cycles and the effectiveness of carbon sequestration (Field et al., 1995; Li et al., 2013; Xie et al., 2014). Traditionally, NPP estimates are based on field surveys, fixed-point observations, or simulations. However, given the limited number of field surveys and the scope of observation, any large-scale, dynamic NPP depiction is effectually impossible. Model simulation is a well-accepted method for estimating terrestrial NPP (Bondeau et al., 1999; Chen et al., 2000; Alexandrov et al., 2002). Process simulation models include BIOM-BGC, SILVAN, TEM, LSM, IBIS, DOLY, and TEM, while production efficiency models include CFix, CFlux, ECLUE, VPRM, two-leaf and CASA (Veroustraete et al., 2002; Xiao et al., 2004; Turner et al., 2006; Yuan et al., 2007; Mahadevan et al., 2008; King et al., 2011; He et al., 2013; Pachavo and Murwira, 2014). There is notable potential for applying remote sensing data based on the CASA model for large-scale, regional NPP simulation (Pachavo and Murwira, 2014). The current version of the CASA model is commonly used for various spatial-temporal NPP estimations (Los et al., 1994; Mao et al., 2012; Zhang et al., 2014a, b, c; Liu et al., 2015). However, model results show a lack of dynamism due to the use of fixed-time land use data.

Terrestrial NPP is highly susceptible to both temperature and precipitation (Yue et al., 2013). However, certain aspects of these relationships are still under debate, owing mainly to variations in the regions and the times that are studied. With respect to the influence of climate factors on terrestrial NPP, precipitation is the dominant factor in low latitudes while temperature is the controlling factor in middle and high latitudes (Gang et al., 2015). The average annual temperature has risen by 1.44°C since the 1960s with a south-to-north gradient alongside an increase in precipitation from the 1960s to the 1990s over China (Fang et al., 2016). NPP in China was on the rise during 1981–2010, Wang et al. (2011) and Pan et al. (2015) argued that NPP is positively correlated with inter-annual average temperature variability respectively in the future and in the first decade of the 21st century, stressing that the dynamic impact of annual average temperature on vegetation is more obvious than that of precipitation. Conversely, Liu et al. (2015) argued that the correlation between NPP and precipitation is stronger than that between NPP and temperature. The extant research has largely centered on spatiotemporal variability in NPP and the impact of climate factors on NPP from the late 20th century onward. However, more in-depth studies on climate elements, spatial-temporal NPP patterns, and correlations among them in the early 2000s are of significant importance.

Raster data with 1-km spatial resolution, including the climate dataset collected from 736 stations across the country, Moderate Resolution Imaging Spectroradiometer (MODIS) monthly vegetation indices, and annual land-cover data, were used to simulate China's NPP via an improved CASA model. Nonparametric methods and spatial-pattern analysis were adopted to test the dynamics and spatial heterogeneity of NPP and climate factors to reveal precise information regarding NPP responses to climate change. We expect that the results discussed below may provide workable knowledge for improving the parameters of the terrestrial ecosystem process model.

2 Data resources

NASA's MODIS Normalized Differential Vegetation Index (NDVI) data (1 km×1 km spatial resolution; 1-month temporal resolution) for the period from January 2001 to December 2013 were used. All data were geometrically and atmospherically corrected, with clouds screened and sensor performance enhanced to ensure consistency and comparability. We also applied chronological series of meteorological data from the China Meteorological Data Network, covering 736 weather stations across the country. The input climate data for the CASA model must be scaled to one month intervals (Fig. 1), so we converted the daily precipitation data (or daily temperature) into monthly data by summing (or averaging) the daily data in each month at each station. We converted daily sunshine duration data into daily and monthly total solar radiation by the same method described by Wang et al. (2017b).

After converting the average temperature, daily precipitation, and sunshine duration into monthly data for the years 2001−2013 at each station, we applied a geographic information system (GIS) interpolation tool for Inverse Distance Weighted (IDW) interpolation of the meteorological data to generate 1 km×1 km raster data with a spatial resolution consistent with NDVI. MODIS land-cover maps

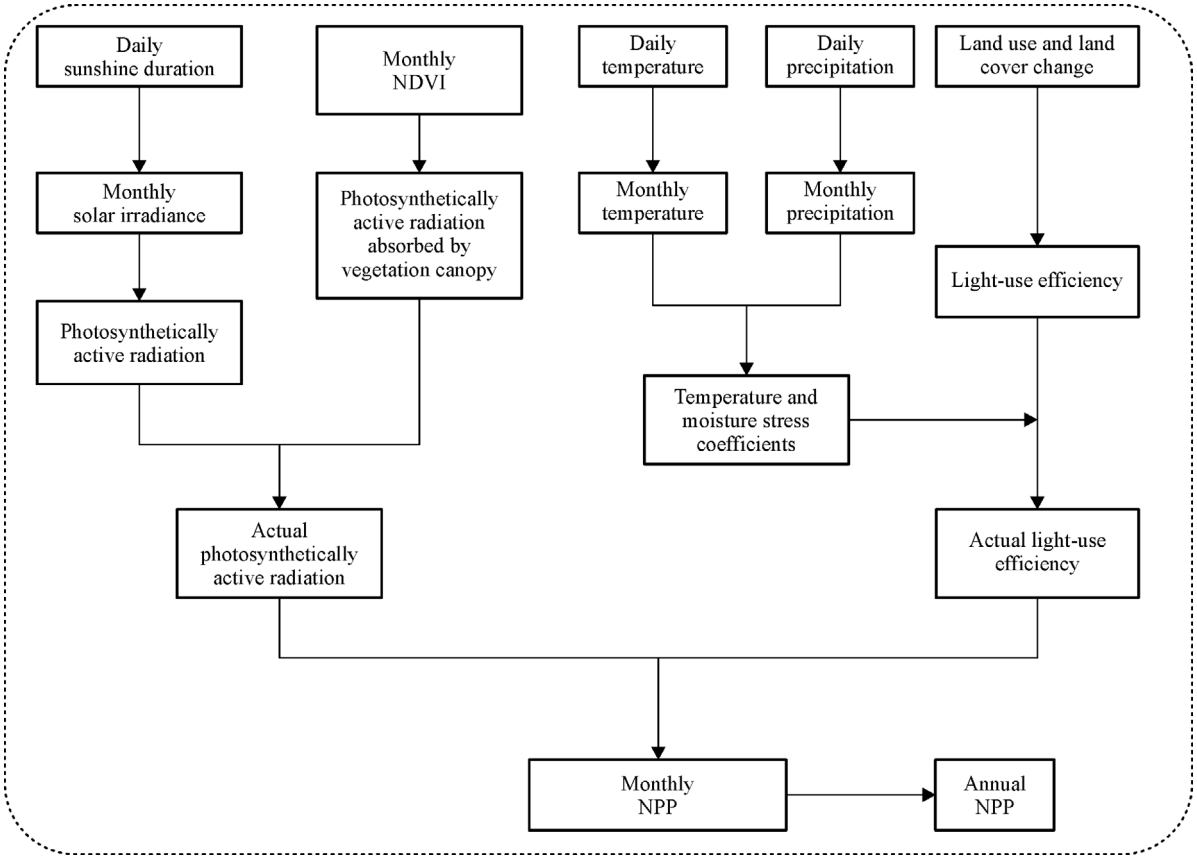

Fig. 1 Improved CASA model simulation generation process.

and MOD12 IGBP land-cover types were used after they were re-sampled to acquire a 1 km×1 km spatial resolution. IGBP classifications offer higher accuracy than other classification products and are, therefore, widely used as input data for land surface models (Ran et al., 2012).

3 Methods

3.1 Improved CASA simulation and NPP estimation

We employed an improved CASA model in this study in which NPP is determined according to absorbed photosynthetically active radiation (APAR) and maximum light utilization efficiency.

$$\mathrm{NPP}_{(x,t)} = \mathrm{APAR}_{(x,t)} * \varepsilon_{(x,t)}, \quad (1)$$

where x is spatial location and t is time, $\mathrm{NPP}_{(x,t)}$ represents the NPP estimate ($\mathrm{gC \cdot m^{-2}}$) at spatial location x and time t in the CASA model, $\mathrm{APAR}_{(x,t)}$ represents the absorbed photosynthetically active radiation at spatial location x and time t, depending on total solar radiation and absorption ratio, and $\varepsilon_{(x,t)}$ represents light use efficiency, i.e., which is the efficiency of converting APAR into organic carbon.

$$\mathrm{APAR}_{(x,t)} = \mathrm{SOL}_{(x,t)} * \mathrm{FPAR}_{(x,t)} * 0.5, \quad (2)$$

where $\mathrm{SOL}_{(x,t)}$ is total solar radiation ($\mathrm{MJ/m^2}$) at spatial location x and time t.

Total solar radiation $\mathrm{SOL}_{(x,t)}$ for Eq. (3) at stations can be obtained by the sunshine duration based on the Ångström function (Jones, 1992). The net shortwave radiation is given by:

$$\mathrm{SOL}_{(x,t)} = \left(a_s + b_s \frac{n}{N}\right) R_a, \quad (3)$$

where $\mathrm{SOL}_{(x,t)}$ is total solar radiation ($\mathrm{MJ \cdot m^{-2} \cdot d^{-1}}$), n is observed sunshine duration at stations (hour), N is potential maximum sunshine duration (hour), R_a is extraterrestrial radiation ($\mathrm{MJ \cdot m^{-2} \cdot d^{-1}}$), and a_s and b_s are constant, respectively 0.25 and 0.5.

The potential maximum sunshine duration (hour) can be calculated by

$$N = \left(\frac{24}{\pi}\right) \omega_s, \quad (4)$$

where ω_s is sunset hour angle expressed in radians (rad); the calculation for ω_s may reference Eq. (6).

The extraterrestrial radiation, R_a for each day of the year and for different latitudes can be estimated from the solar

constant, the solar declination, and the time of the year by:

$$R_a = \frac{24*60}{\pi} G_{sc} d_r [(\omega_s \sin\varphi \sin\delta) + (\cos\varphi \cos\delta \sin\omega_s)], \quad (5)$$

where G_{sc} is solar constant 0.0820 $MJ \cdot m^{-2} \cdot min^{-1}$, d_r is inverse relative distance to Earth-Sun referencing Eq. (7), φ is latitude (rad), and δ is solar declination (rad) which can be obtained by Eq. (8).

$$\omega_s = \arccos[-\tan\varphi \tan\delta], \quad (6)$$

$$d_r = 1 + 0.033\cos\left[\frac{2\pi}{365} J\right], \quad (7)$$

$$\delta = 0.409\sin\left[\frac{2\pi}{365} J - 1.39\right], \quad (8)$$

where J is the number for the day of the year between 1 (1 January) and 365 or 366 (31 December).

$\mathrm{FPAR}_{(x,t)}$ is the fraction of absorbed photosynthetically active radiation at spatial location x and time t, the constant 0.5 represents the proportion of solar radiation (wavelength 0.4 to 0.7 μm) that can be utilized by the vegetation, $\mathrm{FPAR}_{(x,t)}$ varies with normalized difference vegetation index (NDVI) and type of vegetation, and NDVI indicates vegetation coverage, with a maximum value of 0.95, as determined by the following formulas:

$$\mathrm{FPAR}_{(x,t)} = \min\left(\frac{SR_{(x,t)} - SR_{\min}}{SR_{\max} - SR_{\min}}, 0.95\right), \quad (9)$$

$$SR(x,t) = \frac{1 + \mathrm{NDVI}(x,t)}{1 - \mathrm{NDVI}(x,t)}, \quad (10)$$

where $SR_{\min}$ is 1.08; and $SR_{\max}$ depends on type of vegetation and falls between 4.14 and 6.17. The multi-year maximum pixel value of $SR_{(x,t)}$ is used.

$$\varepsilon_{(x,t)} = T\varepsilon 1_{(x,t)} \times T\varepsilon 2_{(x,t)} \times W\varepsilon_{(x,t)} \times \varepsilon_{\max}, \quad (11)$$

$$T\varepsilon 1_{(x,t)} = 0.8 + 0.02 \times T_{opt(x)} - 0.0005 \times [T_{opt(x)}]^2, \quad (12)$$

$$T\varepsilon 2_{(x,t)} = \frac{1.184}{1 + e^{0.2 \times T_{opt(x)} - 10 - T_{(x,t)}}} \times \frac{1}{1 + e^{0.3 \times (-T_{opt(x)}) - 10 + T_{(x,t)}}}, \quad (13)$$

where $\varepsilon_{(x,t)}$ is the actual light use efficiency, depending on several factors (e.g., temperature and moisture), and $\varepsilon_{\max}$ is the maximum light use efficiency under the ideal condition of water, heat, and gas. We set $\varepsilon_{\max}$ values for the different vegetation covers according to the previous publication though the validation of field-observed NPP data at the national scale (Zhu et al., 2006). $T\varepsilon 1_{(x,t)}$ and $T\varepsilon 2_{(x,t)}$ represent temperature coefficients of light use efficiency. Specifically, $T\varepsilon 1_{(x,t)}$ indicates the temperature dependency of the photosynthesis chemical reaction in plants, which is zero when the monthly average temperature is less than or equal to –10°C, and $T\varepsilon 2_{(x,t)}$ indicates the gradual decline trend in photosynthetic efficiency when the ambient temperature deviates from the optimum temperature. $T_{(x,t)}$ is the average temperature (°C) in each month for Eq. (13), $T_{opt(x)}$ represents the average temperature of the month in which the NDVI reaches its peak value over a region in each year; in other words, the referenced optimum temperature.

Cui (2013) proposed calculating procedures for the referenced optimum temperature in seven vegetation-climatic regions, where $W\varepsilon_{(x,t)}$ represents the water stress coefficient determined by the ratio of actual evapotranspiration to potential evapotranspiration. Monthly evapotranspiration values are usually estimated according to monthly total solar radiation, precipitation, and temperature data (Nagler et al., 2007; Brown et al., 2010). $\varepsilon_{\max}$ represents the maximum efficiency of photosynthesis under optimum conditions, which depends on the type of land coverage and varies widely by region. We used MODIS land cover types in this study with reference to the $\varepsilon_{\max}$ parameter in the modified CASA model adopted by Yu et al. (2008), and removed the simulated response of NPP to elevated CO_2 to probe NPP–climate relationships (Piao et al., 2014).

The used CASA model was improved by Zhu et al. (2007), and perfected in three aspects: 1) vegetation cover types were taken into the CASA simulation; 2) according to minimum principia of error in estimating NPP, the maximum light use efficiency for vegetation cover types was simulated based on the field observed data, making the model more suitable to Mainland China; 3) the regional evapotranspiration method was applied to computerize the water stress factor by using the climate data. Refer to the research of Zhu et al. (2007) to obtain more detailed information on the improved CASA model.

3.2 Trend analysis approach

Mann-Kendall (MK) trend analysis is a nonparametric test method (Mann, 1945; Kendall, 1948) which does not require a data series to be normally distributed. The approach is widely used meteorology, ecology, and agricultural research (Burn and Hag Elnur, 2002; Xu et al., 2004). Under the null hypothesis H0, the data series x_k ($k = 1,2,3\ldots,n$) are independent of one another and have the same distribution. Under the alternative hypothesis H1, there is a monotonic trend in the series. The MK test statistics are calculated as follows:

$$S = \sum_{i=1}^{n-1} \sum_{i=j+1}^{n} \mathrm{sgn}(x_j - x_i), \quad (14)$$

where x_j is the sequential data value, n is the length of the dataset, and sgn is calculated as follows:

$$\operatorname{sgn}(x_j - x_i) = \begin{cases} 1 & \text{if } x_j > x_i \\ 0 & \text{if } x_j = x_i \\ -1 & \text{if } x_j < x_i \end{cases}. \quad (15)$$

According to Mann (1945) and Kendall (1948), when $n \geqslant 8$, the test statistics S is approximately normally distributed with the mean and variance:

$$E(S) = 0, \quad (16)$$

$$V(S) = \frac{n(n-1)(2n+5) - \sum_{m=1}^{n} t_m m(m-1)(2m+5)}{18}, \quad (17)$$

where t_m is the value of extent m. The standardized test statistic Z is calculated as follows:

$$Z = \begin{cases} \dfrac{S-1}{\sqrt{V(S)}} & S > 0 \\ 0 & S = 0 \\ \dfrac{S+1}{\sqrt{V(S)}} & S < 0 \end{cases}. \quad (18)$$

$|Z_\alpha|$ = 1.65, 1.96, and 2.58 correspond to the critical values at the significance levels of p = 0.1, 0.05, and 0.01, respectively, if $|Z| > |Z_\alpha|$, H0 is rejected. We used levels p = 0.05 and 0.01 in this study.

To analyze the trend of the time series variable, we used the robust estimator for the amplitude of trend slopes proposed by Sen (1968):

$$\text{slope} = \text{Median}\left(\frac{x_j - x_i}{j-i}\right)(1 \leqslant i < j \leqslant n), \quad (19)$$

where slope is the monotonic increase or decrease rate (or the linear slope) of the entire data series x_k (k = 1,2,3...,n) or any segmentation x_w ($w = i,i+1,i+2...j$). If it is positive, the series monotonically increases; whereas if it is negative, the series monotonically decreases. Median denotes the function of the median value. We performed Sen's trend calculation on the entire series and the segmentations (divided by the results of change-point detection) of annual precipitation data at the stations during the period 1961–2014. A significance test was then conducted on the Sen's trend results using the MK approach.

3.3 Sensitivity analysis

It is important to evaluate the response of NPP to climate factor variability. NPP sensitivity analysis (SA) serves to quantitatively explore the relationship between NPP and temperature (or precipitation). We conducted a sensitivity analysis on precipitation and temperature to NPP by considering the fit linear slope between input variables and output variables as NPP's sensitivity to climate change (Liang et al., 2015). We only evaluated the impact of per-unit climate change on NPP change magnitude, so we used the absolute values of slopes for all the variables in our SA.

In order to further investigate the relationship between NPP and temperature (or precipitation), we assessed NPP sensitivity to climate factors in the 16 vegetation regions according to vegetation cover data. The SA formula is as follows:

$$SA = \frac{\Delta y}{\Delta x} = \frac{\text{slope}(Y)}{\text{slope}(X)}, \quad (20)$$

where SA is the NPP sensitivity value (non-dimensional); Δy and slope(Y) are variations of the output variable (NPP) in the model simulation; and slope(X) and Δx are variations of the input variable (precipitation or temperature) in the model simulation.

4 Results and analysis

4.1 Spatial patterns

Analyzing spatial patterns is a key for identifying hotspots for environmental elements. In this study, we analyzed spatial patterns of China's terrestrial NPP, average annual precipitation, and average annual temperature for the years 2001–2013 to identify the hotspots of different climatic factors.

Spatial patterns of terrestrial NPP in China show distinct spatial heterogeneity (Fig. 2), especially between the southeast and northwest regions of China. The primary types of land cover in northwestern China, include arid and semi-arid areas, sparse vegetation, and grasslands due to very low precipitation, lack of water resources, and high temperatures resulting in a serious desertification problem. Imagine a roughly southwest-to-northeast diagonal line that divides the country into two sections. The section on the west would have NPP values almost entirely below 500 gC/($m^2 \cdot$yr). Alternatively, the main land cover types in the east section would consist of semi-humid and humid areas, agricultural land, and mixed forest with NPP values greater than 500 gC/($m^2 \cdot$yr) or even higher in the coastal areas.

As shown in Fig. 2, very low NPPs prevail in mid-latitude regions with peaks between 38°N and 39°N. As latitude decreases, higher NPP levels emerge across a larger geographical scope. Longitudinally, when roughly divided by a line at 100°E, the section west of the line shows a very low NPP with a peak value near 92°E. NPP increases gradually along the line moving east, reaching a median NPP peak near 116°E.

The spatial distribution of China's annual average

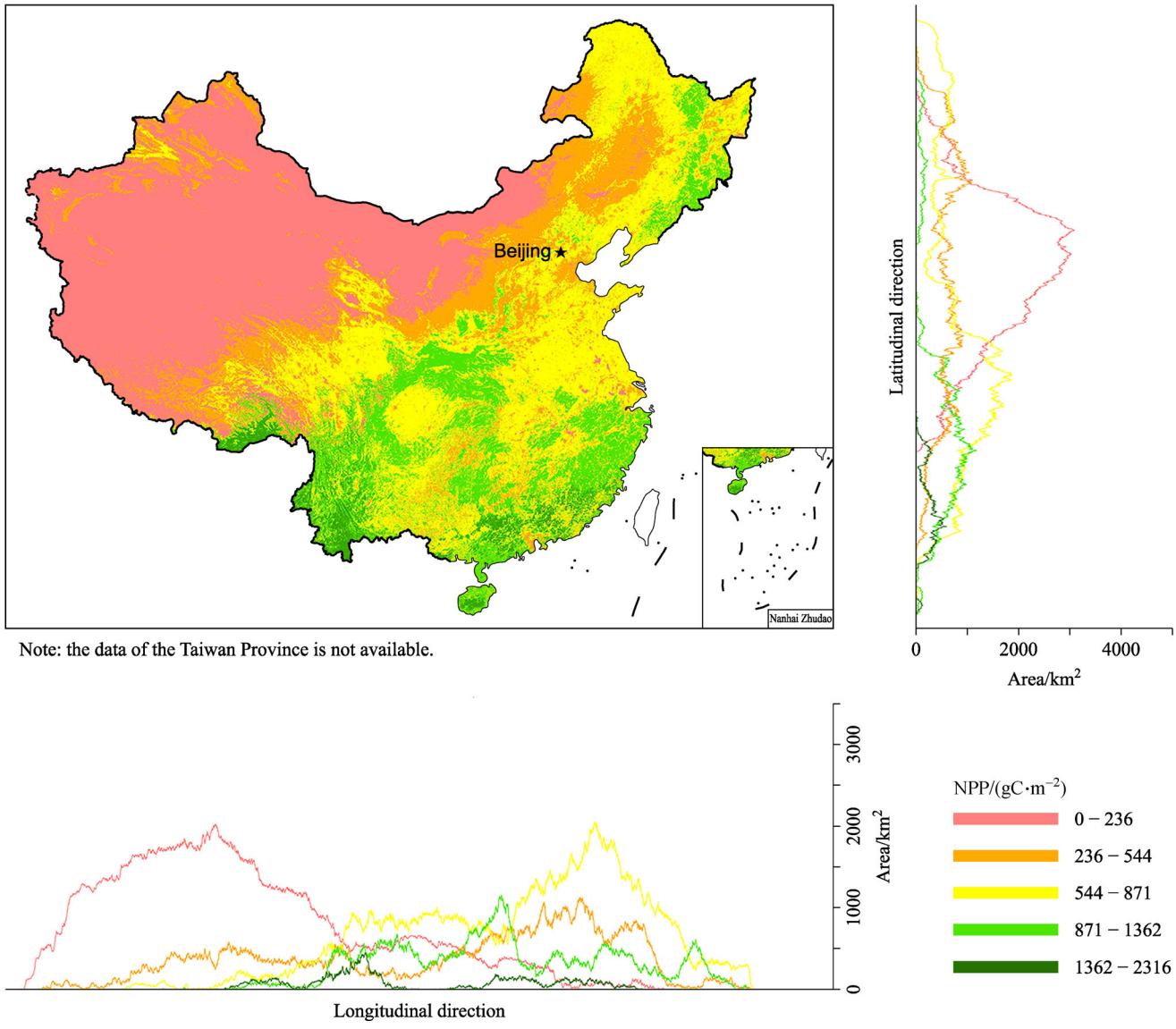

Fig. 2 Spatial patterns of terrestrial NPP in China.

temperature during 2001–2013 is characteristic of distinct latitudinal differences (Fig. 3), the Qinghai-Tibet Plateau and the northern-most reaches of northeastern China are dominated by low temperatures. As indicated in longitudinal and latitudinal directions curve charts, temperature curves alternate as do peak values, owing mainly to the combined impact of altitudes and latitudes on average annual temperature.

The spatial distribution of precipitation in China shows clear and relatively simple spatial differences (Fig. 4). The amount of annual total precipitation varies widely from region to region. There is a ribbon of ragged, progressive decline in the average annual precipitation from the southeast coast to the northwest inland. The amount of total precipitation decreases from south to north and from east to west, as the southeastern part of China is on the coast and the northwestern part extends into the Eurasian continent, very far geographically from the ocean. The annual precipitation generally remains above 1300 mm in the areas south of the Yangtze River and in the southeast coastal areas, owing mainly to their monsoon climate. In longitudinal and latitudinal directions curve charts, low-level curves turn into high-level growth from northwest to southeast. The peak value of low-precipitation curves is approximately 39°N, with multiple peaks in the meridional direction, indicating precipitation variations in both latitudinal and longitudinal directions.

4.2 Spatial trends

Analyzing spatial trends is an important approach to understanding the size or magnitude of variability in

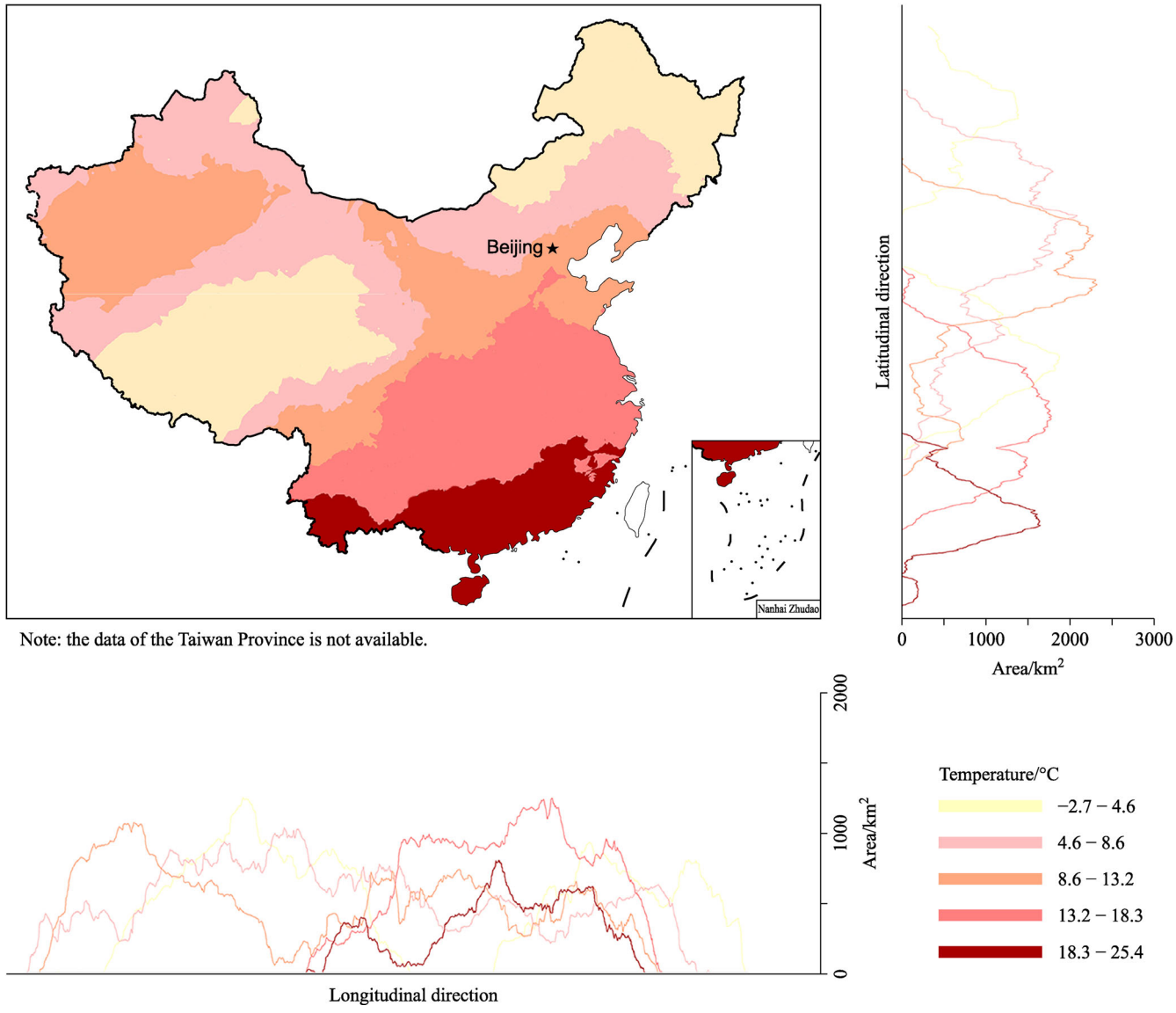

Fig. 3 Spatial patterns of temperature in China.

spatial elements. Again, in this study, our primary focus was spatial trends in China's terrestrial NPP, average annual precipitation, and average annual temperature during 2001–2013 in regions with a greater extent or magnitude of variability than others.

There was little inter-annual variability in China's terrestrial NPP from 2001 to 2013 (Fig. 5), yet there was a significant trend toward NPP increases and positive vegetation growth responses in most parts of the country. As indicated in the spatial distribution map the land areas showing positive NPP changes in northwestern region and the most area in mainland China showed negative NPP changes, especially the decreased trends can be found in eastern and southern regions. The longitudinal and latitudinal directions curve charts also showed the similar trend patterns, in western China, there is a relatively large area showing a negative trend; yet alternatively, a positive trend occurs across a wide swath of eastern China.

The annual average temperature variability over China was spatially clustered during 2001–2013 (Fig. 6). We found a noticeable negative trend in the northeast, especially in the Daxing'anling Prefecture. The downward trend grew less severe in the southwesterly direction, reflective of a mild decline in temperature without significant changes in the region. In southwestern China, temperature increased overall during the study period, especially in the central parts of Tibet and most of Yunnan. Longitudinal and latitudinal directions curve charts show similar change.

Precipitation over China was spatially "patchy" during 2001−2013 (Fig. 7), indicative of an increase in precipitation in most parts of the country; yet there was a marked

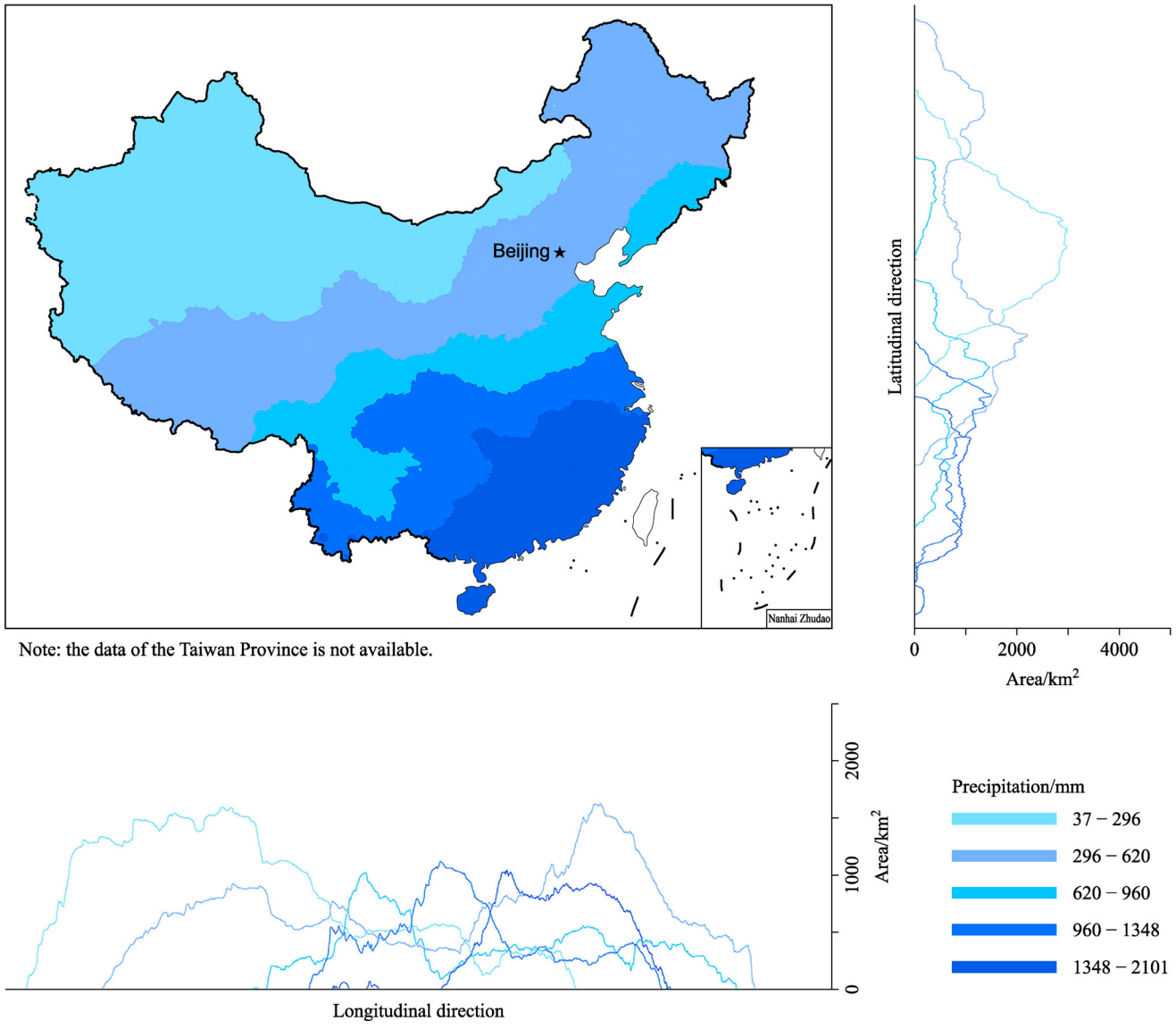

Fig. 4 Spatial patterns of precipitation in China.

decrease in central and southwestern China and a less dramatic decrease in northwestern China. A remarkable increase occurred in the areas surrounding the Qiongzhou Strait, with the amount of year-to-year variability up to 50 mm. The most visible decline was in central Yunnan, with year-to-year variability up to 20 mm. A significant increase in total precipitation occurred in northeastern China, accompanied by a downward trend in southern Inner Mongolia, central Tibet, some parts of Xinjiang, and some coastal areas in Guangdong. Water shortage continually worsened over the study area in northwestern China.

4.3 Spatial correlation properties

A spatial correlation analysis measures the interaction between two spatial elements. In this study, we analyzed the correlations of China's terrestrial NPP with two climatic factors, average precipitation and average annual temperature.

We found no significant correlation between NPP and average annual temperature (Fig. 8). As indicated in longitudinal and latitudinal directions curve charts, an insignificant correlation accounts for a much greater area ($p > 0.05$) when compared to other degrees of correlation. A negative correlation between NPP and average annual temperature is scattered across northern China, indicating that changes in temperature from 2000–2013 had little impact on NPP. In the northeastern section of Qinghai-Tibet Plateau, the positive correlation between NPP and average annual temperature was significant. That is, increases in temperature due to climate warming had a positive impact on NPP, contributing to vegetation growth

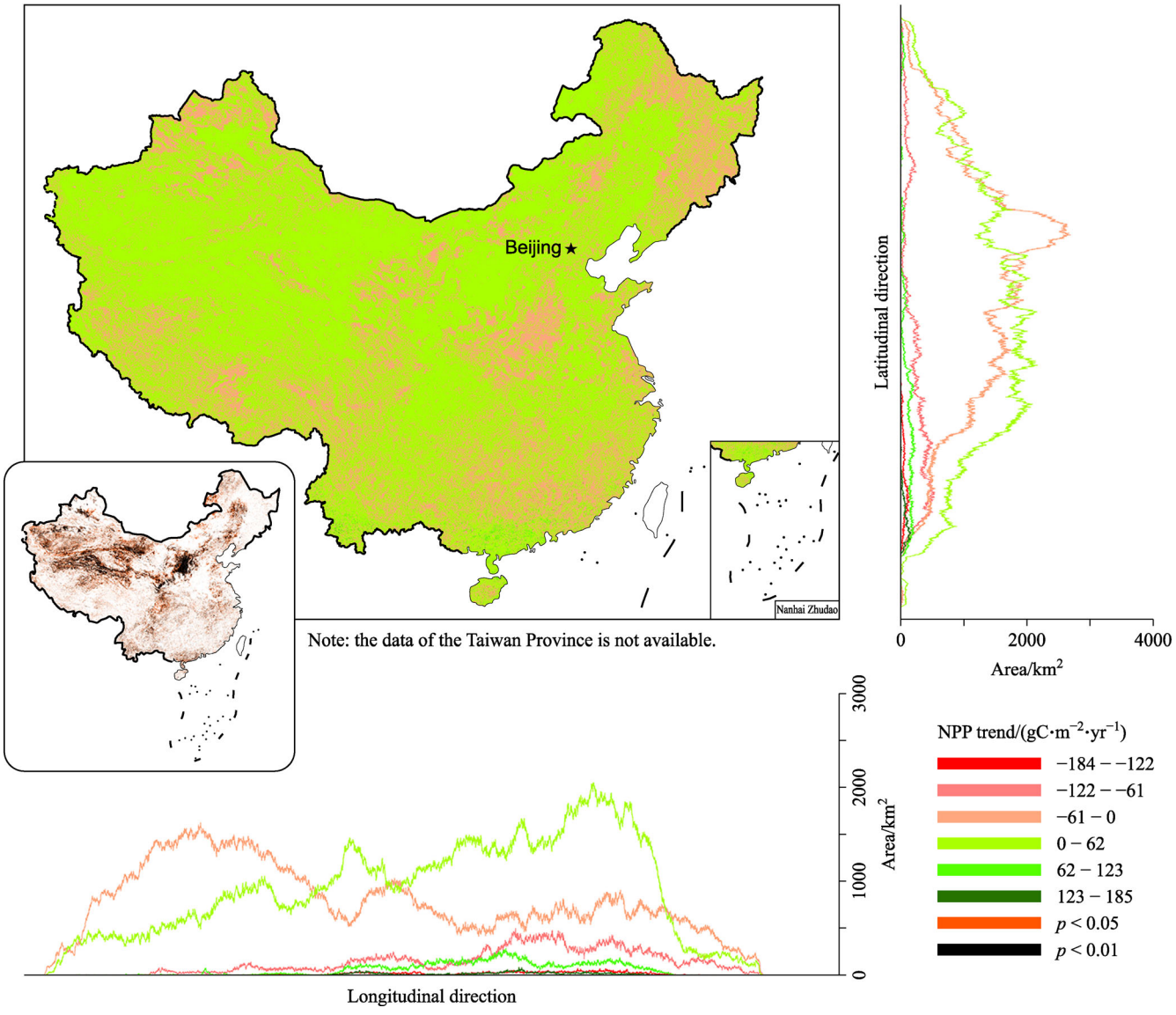

Fig. 5 Spatial trends of terrestrial NPP in China. The small inset map in Fig. 5 shows that the spatial pattern of trend significance levels marked by "*p*". The region filled in white is non-significant at $p > 0.05$.

in this region.

We observed a stronger correlation in northern region between NPP and precipitation compared to that between NPP and temperature (Fig. 9), indicating that changes in precipitation had a greater impact on NPP across China throughout the study period. In particular, the correlation efficient above 0.64 in northern and central China is significant. Our significance test results ($p < 0.01$) show that the increase in precipitation in this region contributed to the growth of vegetation and emergence of more absorbent plants. However, NPP is negatively correlated with precipitation in the eastern part of the Qinghai-Tibet Plateau and Sichuan Basin, indicating that an increase in precipitation contributed to soil respiration and inhibited plant growth. Our longitudinal and latitudinal directions curve charts reveal an insignificant correlation between NPP and precipitation across most regions of the country excepting northern region.

5 Discussion

Accurately evaluating the impact of climate factors on NPP is useful for conducting meaningful SA of NPP to temperature and precipitation. NPP is one of the most important parameters indicating the carbon budget of regional vegetation. The sensitivity of NPP to climate factors may vary across regions with different vegetation cover.

Our SA result for NPP and climate factors related to 16

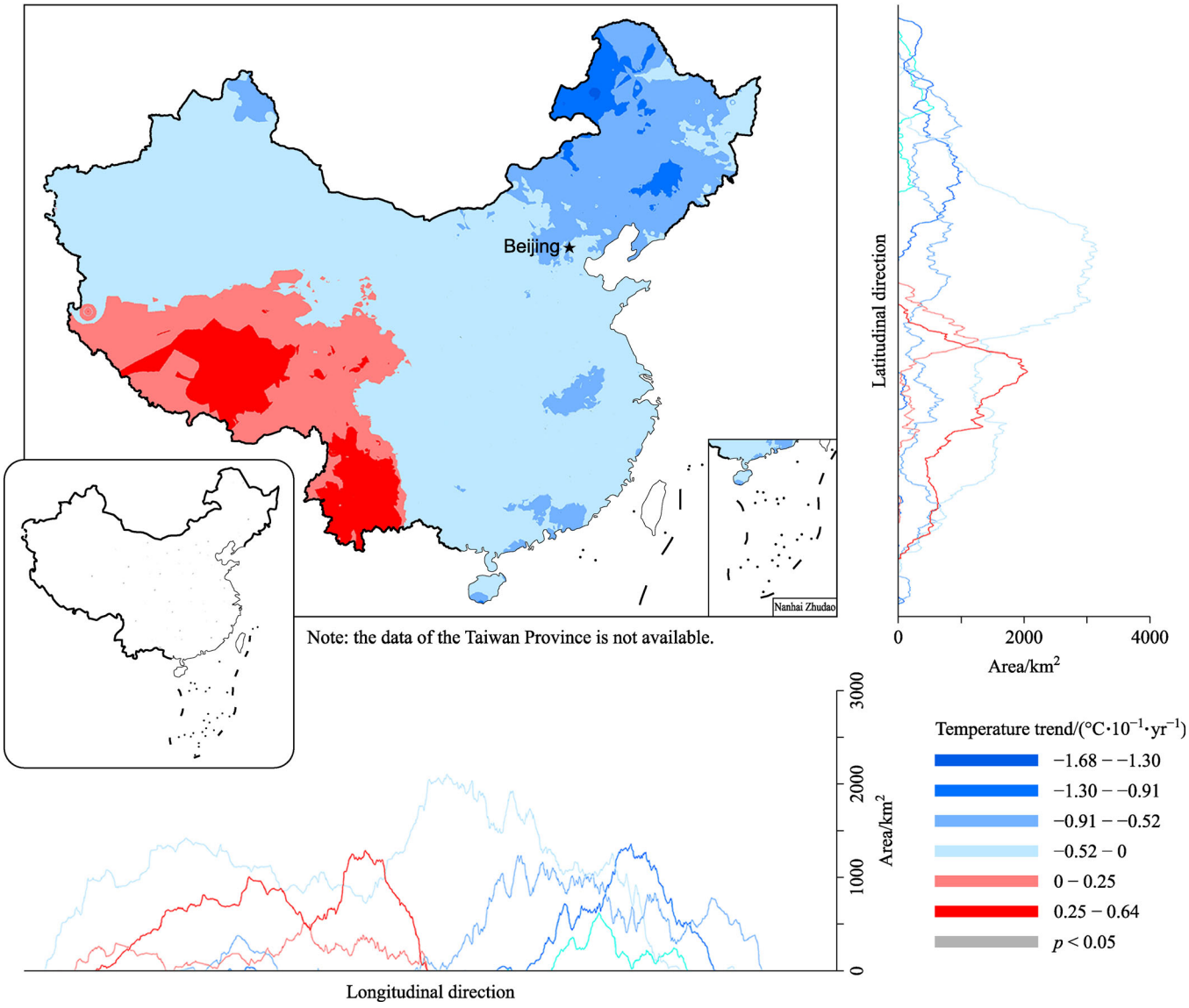

Fig. 6 Spatial patterns of temperature variability in China. The small inset map in Fig. 6 shows the spatial pattern of trend significance levels marked by "*p*". The region filled in white is non-significant at $p > 0.05$).

vegetation types is shown in Table 1, where the values of NPP SA to precipitation vary from 0.98 to 78.86 across the various regions. The values are maximum in needleleaf deciduous forest type and minimum in broadleaf evergreen forest type. China's broadleaf evergreen forest lies within a humid region where precipitation is not the main limiting factor for vegetation growth. Conversely, the country's needleleaf deciduous forest is mainly distributed in an alpine zone where precipitation limits growth considerably.

The values of NPP SA to temperature vary from 217 to 3333 across all the vegetation regions we tested. The values are maximum in wetland type and minimum in needleleaf evergreen forest type. The values of NPP SA to temperature are much higher than that of NPP SA to precipitation. In other words, any change in per-unit temperature had a more severe impact on NPP than the change in per-unit precipitation. However, NPP is indeed sensitive to both precipitation and temperature in all 16 vegetation types. To this effect, the proposed model reveals the effects of precipitation and temperature on NPP.

The NPP SA indicates that there is a variance on the impact of climate factors on NPP for different vegetation types. NPP is currently estimated using three types of models to include a climate productivity model (Miami model), terrestrial ecosystem process model (BIOME-BGC model, CENTURY model, and TEM model) and a light utilization efficiency model (CASA). The CASA model is suitable for research at larger spatial scales. Even though ecological and physiological mechanisms of

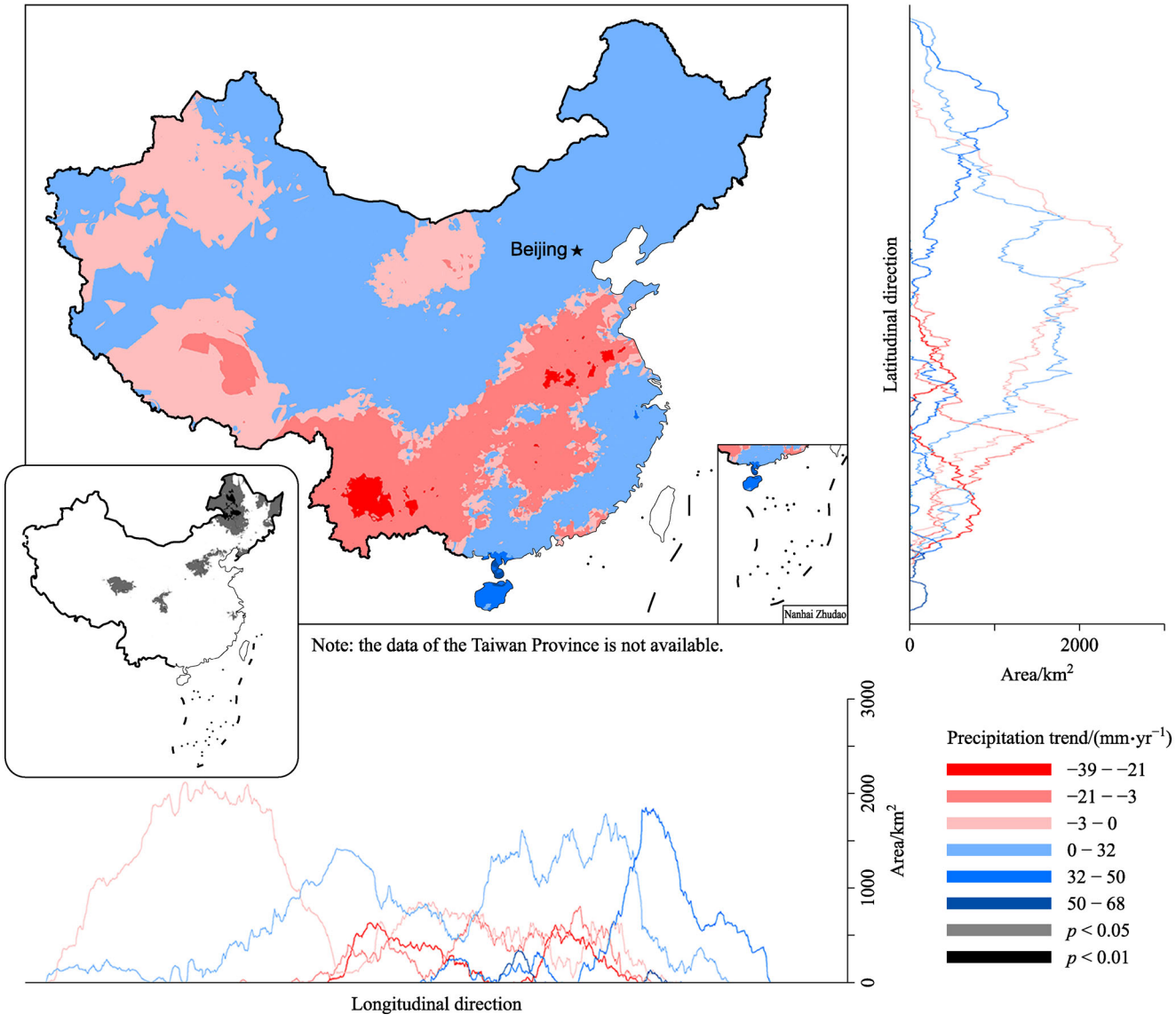

Fig. 7 Spatial patterns of precipitation variability in China. The small inset map in Fig. 7 shows the spatial pattern of trend significance levels marked by "*p*". The region filled in white is non-significant at $p > 0.05$).

CASA are unclear for vegetation growth, it can accurately estimate NPP without diurnal vegetation growth parameters; however, the terrestrial ecosystem process model with simulating diurnal growth parameters can be perfected or improved by assimilating and adopting some reliable research conclusions on relationships between climatic-environmental factors and NPP. The NPP SA and analysis in relationships between precipitation (or temperature) and NPP can provide useful information for improving calibration parameters of the terrestrial ecosystem process model.

The spatial trends in terrestrial NPP in China increased in the north and decreased in the south due to the increases in NPP over northern China, which were offset by NPP decreases over the more productive forested regions of southern China (Wang et al., 2017a). These results are consistent with previously published long-term trend analyses, which suggest that the NPP for the whole region of China increased over the past two decades (Cao et al., 2003). Annual mean air temperatures decreased in North China, but increased in Southwest China during 2001–2013. These phenomena are consistent with previous research conclusions stating that global surface temperatures did not rise between 1998 and 2008 due to a global warming hiatus. This hiatus in warming coincided with a period of relatively little increase in the sum of anthropogenic and natural forces (Kaufmann et al., 2011). Our results also support the prediction that the world's climate

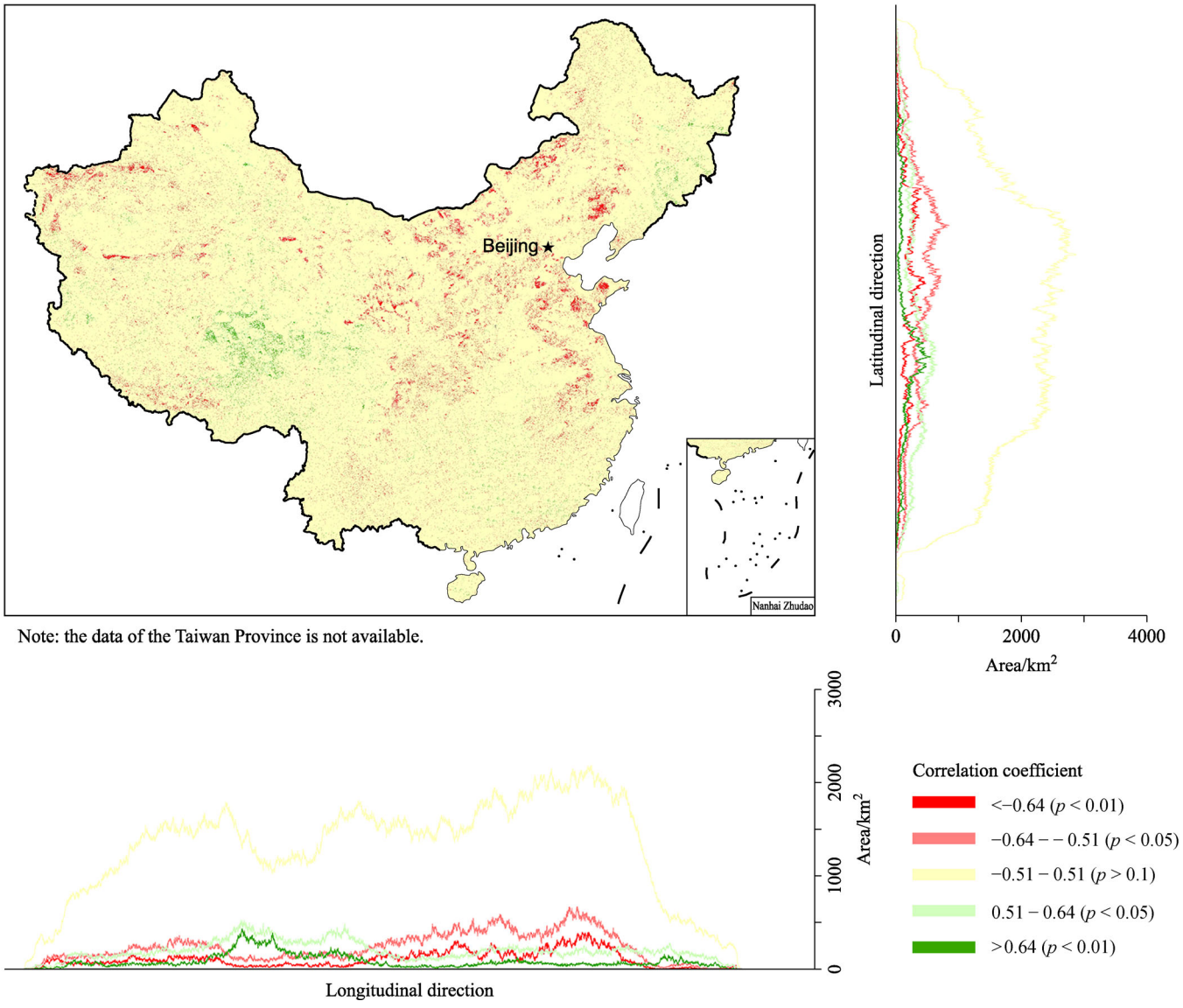

Fig. 8 Spatial correlation between NPP and temperature.

will produce periods of a decade or two where the globally averaged surface air temperature shows no trend or even slight cooling in the presence of longer-term warming over the 21th century (Easterling and Wehner, 2009). The annual total precipitation trends we observed over China during 2001 to 2013 are also similar to previously identified trends from between 1999 and 2010 (Liang et al., 2015).

In our study, the simple method was used to investigate the relationships between climate factors and NPP (Zhao and Running, 2010). This method can dynamically assess and predict the response of NPP to climate change (or impact of climate change on NPP) for a specific period of time. For the hiatus in warming, there is little effect of air temperature on the NPP of vegetation over China, which is a significant conclusion that supports related research on vegetation ecology and the carbon cycle. This conclusion is also one of novelty points in this study. The vegetation coverage types are assumed in a fixed year with unchanged conditions from previous studies (Zhu et al., 2007; Zhao and Running, 2010). For a more accurate estimation, we employed the actual vegetation coverage types in each year, which is the second novelty point of this study. To better express the spatial characteristics at the national scale with a longitudinal and latitudinal consideration, the method of results is conducted by combining the spatial pattern maps and variations diagram in two directions, which is the third novelty point of this study.

The results reported here may help to elucidate vegetation responses to climatic factors within the first 13 years of the 21st century. We assume that they will also provide a workable knowledge for improving the para-

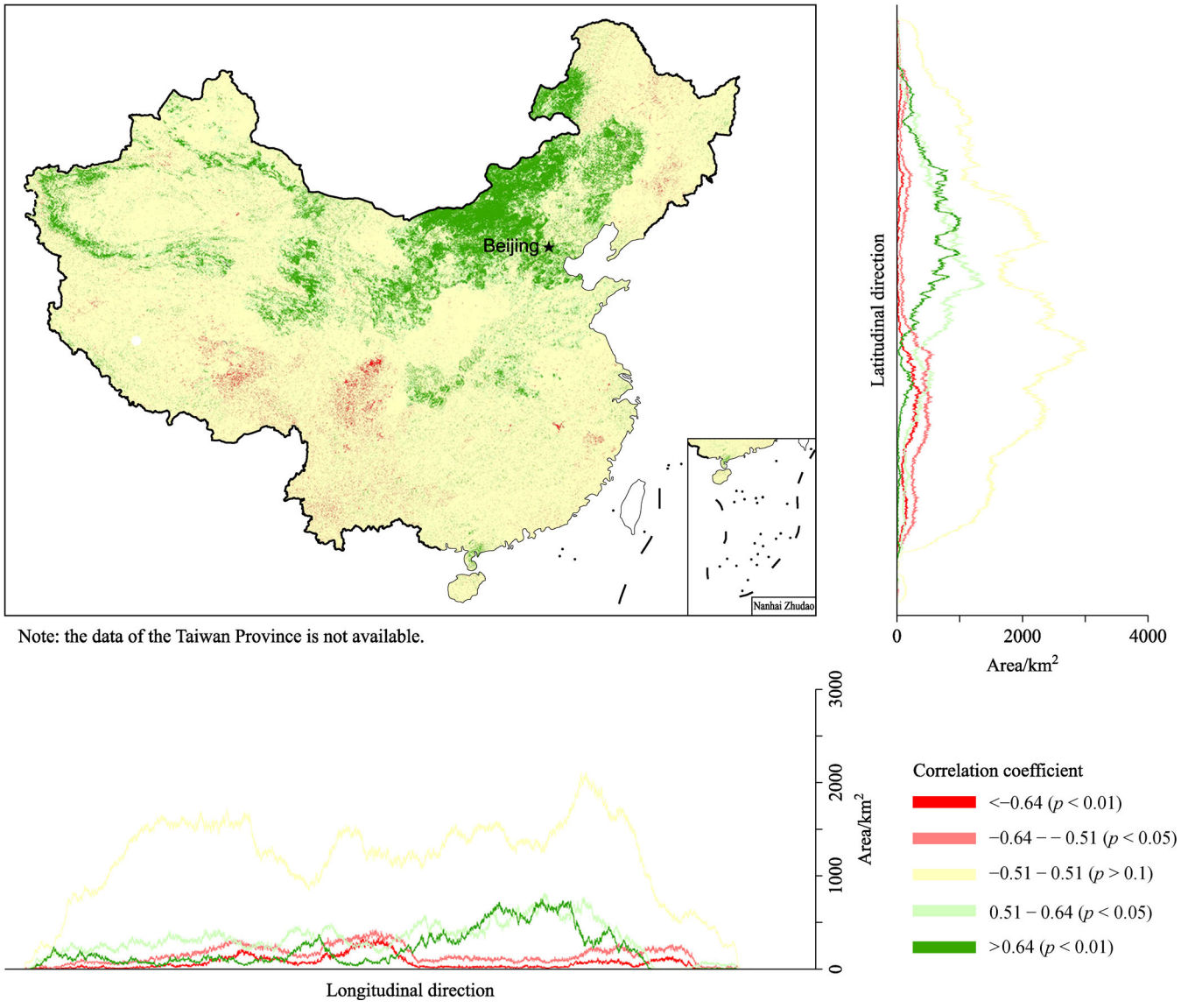

Fig. 9 Spatial correlation between NPP and precipitation.

meters of the terrestrial ecosystem process model. Further research is yet necessary to reveal how various types of vegetation, topographic factors, or other environmental elements influence plant growth. The dynamic characteristics of NPP should also be investigated further within specific land cover types and different regions.

6 Conclusions

NPP, an important vegetation parameter and ecological indicator, can facilitate clear visualization in ecological environments and regional carbon budgets across the globe. In our study, we employed an improved CASA model to simulate China's NPP at the grid scale, taking into account the land-cover variables and the maximum photosynthetic efficiency of vegetation for several different land cover types. We explored the grid-based characteristics of spatial patterns and dynamics of NPP, annual temperature, and annual precipitation. Our conclusions can be summarized as follows.

The spatial distribution of China's NPP, on the whole, is characterized by "higher values in the southeast and lower values in the northwest." The spatial distribution of temperatures is indicative of remarkable latitudinal differences while the spatial distribution of precipitation shows "a ribbon of progressive decline from the southeast coast to the northwest inland."

An upward trend in China's terrestrial NPP was visible in most parts of the country. China's average annual temperature variability is spatially clustered, with a noticeable negative trend in the northeast. China's

Table 1 SA on NPP and climate factors

Vegetation type	Precipitation (SA)	Temperature (SA)
Broadleaf evergreen forest	0.98	1666
Broadleaf deciduous forest	1.58	218
Needleleaf evergreen forest	3.21	217
Needleleaf deciduous forest	78.86	1474
Mixed forest	12.38	802
Tree open	4.05	763
Shrub	3.45	582
Herbaceous	11.06	667
Herbaceous with Sparse Tree/Shrub	3.91	526
Sparse vegetation	8.88	1626
Cropland	8.37	914
Paddy field	8.28	1616
Cropland/other vegetation mosaic	18.88	1919
Mangrove	9.86	929
Wetland	3.00	3333

precipitation is spatially patchy, with an increase in most parts of the country and a noticeable decline in central and southwestern areas.

We found that NPP is not significantly correlated with average annual temperatures. There is a negative correlation between NPP and average annual temperatures in northern China. Variability in temperature had little impact on NPP during 2001−2013. NPP and annual precipitation are positively correlated in northern and central China with a correlation coefficient above 0.64 ($p < 0.01$) and negatively correlated in the eastern parts of the Qinghai-Tibet Plateau and the Sichuan Basin.

Acknowledgements This research received financial support from the National Basic Research Program of China (No. 2016YFC0502900), the National Natural Science Foundation of China (Nos. 41601562, 41401643, and 41401050), the Research Project for Young Teachers of Fujian Province (No. JAT160085), and the Scientific Research Foundation of Fuzhou University (No. XRC-1536). We would like to thank the editors and reviewers for providing helpful suggestions and support.

References

Alexandrov G, Oikawa T, Yamagata Y (2002). The scheme for globalization of a process-based model explaining gradations in terrestrial NPP and its application. Ecol Modell, 148(3): 293–306

Bondeau A, Kicklighter D W, Kaduk J, the Participants of the Potsdam NPP model intercomparison (1999). Comparing global models of terrestrial net primary productivity (NPP): importance of vegetation structure on seasonal NPP estimates. Glob Change Biol, 5(S1): 35–45

Brown S M, Petrone R M, Mendoza C, Devito K J (2010). Surface vegetation controls on evapotranspiration from a sub-humid Western Boreal Plain wetland. Hydrol Processes, 24(8): 1072–1085

Burn D H, Hag Elnur M A (2002). Detection of hydrologic trends and variability. J Hydrol (Amst), 255(1–4): 107–122

Cao M, Tao B, Li K, Shao X, Stephen D (2003). Interannual variation in terrestrial ecosystem carbon fluxes in China from 1981 to 1998. Acta Bot Sin, 45(5): 552–560

Cao M, Woodward F I (1998). Dynamic responses of terrestrial ecosystem carbon cycling to global climate change. Nature, 393 (6682): 249–252

Chandrappa R, Gupta S, Kulshrestha U C (2011). Industrial Revolutions, Climate Change and Asia, Coping with Climate Change. Berlin: Springer

Chen L, Liu G, Feng X (2000). Estimation of net primary productivity of terrestrial vegetation in China by remote sensing. Acta Bot Sin, 43 (11): 1191–1198

Crabtree R, Potter C, Mullen R, Sheldon J, Huang S, Harmsen J, Rodman A, Jean C (2009). A modeling and spatio-temporal analysis framework for monitoring environmental change using NPP as an ecosystem indicator. Remote Sens Environ, 113(7): 1486–1496

Cui Y (2013). Preliminary estimation of the realistic optimum temperature for vegetation growth in China. Environ Manage, 52 (1): 151–162

Dong M, Yu M (2008). Simulation analysis on net primary productivity of grassland communities along a water gradient and their responses to climate change. J Plant Ecol, 32(3): 531–543

Easterling D R, Wehner M F (2009). Is the climate warming or cooling? Geophys Res Lett, 36(8): L08706

Fang O, Wang Y, Shao X (2016). The effect of climate on the net primary productivity (NPP) of *Pinus koraiensis* in the Changbai Mountains over the past 50 years. Trees (Berl), 30(1): 281–294

Field C B, Randerson J T, Malmström C M (1995). Global net primary production: combining ecology and remote sensing. Remote Sens Environ, 51(1): 74–88

Gang C, Zhang Y, Wang Z, Chen Y, Yang Y, Li J, Cheng J, Qi J, Odeh I (2017). Modeling the dynamics of distribution, extent, and NPP of global terrestrial ecosystems in response to future climate change. Global Planet Change, 148: 153–165

Gang C, Zhou W, Wang Z, Chen Y, Li J, Chen J, Qi J, Odeh I, Groisman P (2015). Comparative assessment of grassland NPP dynamics in response to climate change in China, North America, Europe and Australia from 1981 to 2010. J Agron Crop Sci, 201(1): 57–68

He M, Ju W, Zhou Y, Chen J, He H, Wang S, Wang H, Guan D, Yan J, Li Y, Hao Y, Zhao F (2013). Development of a two-leaf light use efficiency model for improving the calculation of terrestrial gross primary productivity. Agric Meteorol, 173: 28–39

Jones H G (1992). Plant and Microclimate. A Quantitative Approach to Environmental Plant Physiology (2nd ed). Cambridge University Press

Kaufmann R K, Kauppi H, Mann M L, Stock J H (2011). Reconciling anthropogenic climate change with observed temperature 1998–2008. Proc Natl Acad Sci USA, 108(29): 11790–11793

Kendall M G (1948). Rank Correlation Methods. London: Charles Griffin

King D A, Turner D P, Ritts W D (2011). Parameterization of a diagnostic carbon cycle model for continental scale application. Remote Sens Environ, 115(7): 1653–1664

Li J, Cui Y, Liu J, Shi W, Qin Y (2013). Estimation and analysis of net primary productivity by integrating MODIS remote sensing data with a light use efficiency model. Ecol Modell, 252(1): 3–10

Liang W, Yang Y T, Fan D M, Guan H D, Zhang T, Long D, Zhou Y, Bai D (2015). Analysis of spatial and temporal patterns of net primary production and their climate controls in China from 1982 to 2010. Agric Meteorol, 204: 22–36

Liu C, Dong X, Liu Y (2015). Changes of NPP and their relationship to climate factors based on the transformation of different scales in Gansu, China. Catena, 125: 190–199

Los S O, Justice C, Tucker C (1994). A global 1° by 1° NDVI data set for climate studies derived from the GIMMS continental NDVI data. Int J Remote Sens, 15(17): 3493–3518

Mahadevan P, Wofsy S C, Matross D M, Xiao X, Dunn A L, Lin J C, Gerbig C, Munger J W, Chow V Y, Gottlieb E W (2008). A satellite-based biosphere parameterization for net ecosystem CO_2 exchange: vegetation photosynthesis and respiration model (VPRM). Global Biogeochem Cycles, 22(2): GB2005

Mann H B (1945). Nonparametric tests against trend. Econometrica, 13 (3): 245–259

Mao D, Wang Z, Han J, Ren C (2012). Spatio-temporal pattern of net primary productivity and its driven factors in Northeast China in 1982–2010. Scientia Geographica Sinica, 32: 1106–1111

Nagler P L, Glenn E P, Kim H, Emmerich W, Scott R L, Huxman T E, Huete A R (2007). Relationship between evapotranspiration and precipitation pulses in a semiarid rangeland estimated by moisture flux towers and MODIS vegetation indices. J Arid Environ, 70(3): 443–462

Nemani R R, Keeling C D, Hashimoto H, Jolly W M, Piper S C, Tucker C J, Myneni R B, Running S W (2003). Climate-driven increases in global terrestrial net primary production from 1982 to 1999. Science, 300(5625): 1560–1563

Olesen J E, Carter T, Diaz-Ambrona C, Fronzek S, Heidmann T, Hickler T, Holt T, Minguez M, Morales P, Palutikof J, Quemada M, Ruiz-Ramos M, Rubæk G H, Sau F, Smith B, Sykes M T (2007). Uncertainties in projected impacts of climate change on European agriculture and terrestrial ecosystems based on scenarios from regional climate models. Clim Change, 81(S1): 123–143

Pachauri R K, Allen M R, Barros V R, Broome J, Cramer W, Christ R, Church J A, Clarke L, Dahe Q, Dasgupta P (2014). IPCC, Climate Change 2014: Synthesis Report, Contribution of Working Groups I, II and III to the Fifth Assessment Report of the Intergovernmental Panel on Climate Change (Intergovernmental Panel on Climate Change, 2014), 1–151

Pachavo G, Murwira A (2014). Remote sensing net primary productivity (NPP) estimation with the aid of GIS modelled shortwave radiation (SWR) in a Southern African Savanna. Int J Appl Earth Obs Geoinf, 30(1): 217–226

Palut M P, Canziani O F (2007). Contribution of Working Group II to the Fourth Assessment Report of the Intergovernmental Panel on Climate Change. Cambridge University Press

Pan S, Tian H, Dangal S R, Ouyang Z, Lu C, Yang J, Tao B, Ren W, Banger K, Yang Q, Zhang B (2015). Impacts of climate variability and extremes on global net primary production in the first decade of the 21st century. J Geogr Sci, 25(9): 1027–1044

Piao S, Ciais P, Friedlingstein P, Peylin P, Reichstein M, Luyssaert S, Margolis H, Fang J, Barr A, Chen A, Grelle A, Hollinger D Y, Laurila T, Lindroth A, Richardson A D, Vesala T (2008). Net carbon dioxide losses of northern ecosystems in response to autumn warming. Nature, 451(7174): 49–52

Piao S, Nan H, Huntingford C, Ciais P, Friedlingstein P, Sitch S, Peng S, Ahlstrom Am Canadell J G, Cong N, Levis S, Levy P E, Liu L, Lomas M R, Mao J, Myneni R B, Peylin P, Poulter B, Shi X, Yin G, Viovy N, Wang T, Wang X, Zaehle S, Zeng N, Zeng Z, Chen A (2014). Evidence for a weakening relationship between interannual temperature variability and northern vegetation activity. Nat Commun, 5(5018): 1–7

Ran Y, Li X, Lu L, Li Z (2012). Large-scale land cover mapping with the integration of multi-source information based on the Dempster–Shafer theory. Int J Geogr Inf Sci, 26(1): 169–191

Running S W, Nemani R R, Heinsch F A, Zhao M, Reeves M, Hashimoto H (2004). A continuous satellite-derived measure of global terrestrial primary production. Bioscience, 54(6): 547–560

Sen P K (1968). Estimates of the regression coefficient based on Kendall's Tau. J Am Stat Assoc, 63(324): 1379–1389

Turner D, Ritts W, Styles J, Yang Z, Cohen W, Law B, Thornton P (2006). A diagnostic carbon flux model to monitor the effects of disturbance and interannual variation in climate on regional NEP. Tellus B Chem Phys Meterol, 58(5): 476–490

Veroustraete F, Sabbe H, Eerens H (2002). Estimation of carbon mass fluxes over Europe using the C-Fix model and Euroflux data. Remote Sens Environ, 83(3): 376–399

Wang F, Xu Y J, Dean T J (2011). Projecting climate change effects on forest net primary productivity in subtropical Louisiana, USA. Ambio, 40(5): 506–520

Wang J, Dong J, Yi Y, Lu G, Oyler J, Simth W K, Zhao M, Liu J, Running S (2017a). Decreasing net primary production due to drought and slight decreases in solar radiation in China from 2000 to 2012. J Geophys Res, 122(1), doi: 10.1002/2016JG003417

Wang Q, Wu J, Li X, Zhou H, Yang J, Geng G, An X, Liu L, Tang Z (2017b). A comprehensively quantitative method of evaluating the impact of drought on crop yield using daily multi-scale SPEI and crop growth process model. Int J Biometeorol, 61(4): 685–699

Xiao X, Hollinger D, Aber J, Goltz M, Davidson E A, Zhang Q, Moore B III (2004). Satellite-based modeling of gross primary production in an evergreen needleleaf forest. Remote Sens Environ, 89(4): 519–534

Xie B, Qin Z, Wang Y, Chang Q (2014). Spatial and temporal variation in terrestrial net primary productivity on Chinese Loess Plateau and its influential factors. Transactions of the Chinese society of Agricultural Engineering, 30(11): 244–253

Xu Z, Chen Y, Li J (2004). Impact of climate change on water resources in the Tarim River basin. Water Resour Manage, 18(5): 439–458

Yu D, Zhu W, Pan Y (2008). The role of atmospheric circulation system playing in coupling relationship between spring NPP and precipitation in East Asia area. Environ Monit Assess, 145(1–3): 135–143

Yuan W, Liu S, Zhou G, Zhou G, Tieszen L L, Baldocchi D, Bernhofer C, Gholz H, Goldstein A H, Goulden M L, Hollinger D Y, Hu Y, Law B E, Stoy P C, Vesala T, Wofsy S C (2007). Deriving a light use efficiency model from eddy covariance flux data for predicting daily gross primary production across biomes. Agric Meteorol, 143(3–4): 189–207

Yue T X, Zhao N, Ramsey R D, Wang C L, Fan Z M, Chen C F, Lu Y M,

Li B L (2013). Climate change trend in China, with improved accuracy. Clim Change, 120(1−2): 137–151

Zhang F, Feng Q, Li X, Wei Y (2014a). Remotely-sensed estimation of NPP and its spatial-temporal characteristics in the Heihe River Basin. J Desert Res, 34: 1657–1664

Zhang Y, Jia W, Zhao Y, Liu Y, Zhao Z, Chen J (2014b). Spatial-temporal variations of net primary productivity of Qilian mountains vegetation based on CASA model. Acta Botanica Boreali-Occidentalia Sinica, 34: 2085–2091

Zhang Y, Qi W, Zhou C, Ding M, Liu L, Gao J, Bai W, Wang Z, Zheng D (2014c). Spatial and temporal variability in the net primary production of alpine grassland on the Tibetan Plateau since 1982. J Geogr Sci, 24(2): 269–287

Zhao M, Running S (2010). Drought-induced reduction in global terrestrial net primary production from 2000 through 2009. Science, 329(5994): 940–943

Zhu W, Pan Y, He H, Yu D, Hu H (2006). Simulation of maximum light use efficiency for some typical vegetation types in China. Chin Sci Bull, 51(4): 457–463

Zhu W, Pan Y, Zhang J (2007). Estimation of net primary productivity of Chinese terrestrial vegetation based on remote sensing. J Plant Ecol, 31(3): 413–424